Nanoparticle Superlattices with Negative Thermal Expansion (NTE) Coefficients

Hyeong Jin Kim,[†] Wenjie Wang,[‡] Surya Mallapragada,[†] Alex Travesset,[*,¶] and David Vaknin[*,¶]

[†]*Ames Laboratory, and Department of Chemical and Biological Engineering, Iowa State University, Ames, Iowa 50011, USA*
[‡]*Division of Materials Sciences and Engineering, Ames Laboratory, U.S. DOE, Ames, Iowa 50011, USA*
[¶]*Ames Laboratory, and Department of Physics and Astronomy, Iowa State University, Ames, Iowa 50011, USA*

E-mail: trvsst@ameslab.gov; vaknin@ameslab.gov

Abstract

We report on the assembly of gold nanoparticles grafted with polyethylene glycol (PEG-AuNPs) in aqueous solutions into the face centered cubic superlattice by synchrotron X-ray scattering. At sufficiently high salt concentrations, the lattice constant decreases with increasing temperature, *i.e.* it exhibits a negative thermal expansion (NTE) coefficient that is two to four orders (in magnitude) larger than previously reported in NTE materials. The generality of the effect is demonstrated with different salts and different PEG chain lengths. Theoretical calculations show that PEG-AuNP becomes more insoluble (with the Flory-Huggins parameter $\chi > \frac{1}{2}$), as temperature increases through water dehydration, with a decrease in volume of the superlattice and an increase in the entropy of the system. Implications on the formation of nanoparticle superlattices and NTE properties are also discussed.

Keywords

gold nanoparticles; assembling nanoparticles; negative thermal expansion; peg-grafted gold nanoparticle; small-angle x-ray scattering (saxs)

TOC

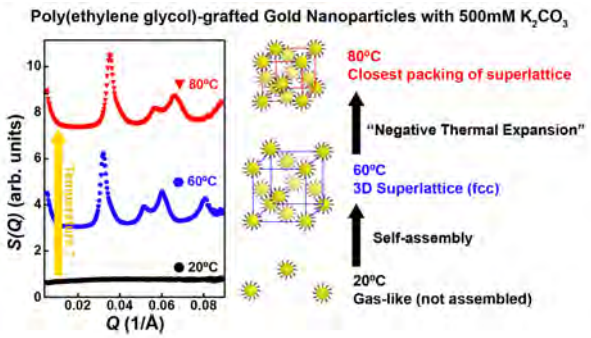

Introduction

Polyethylene Glycol (PEG) displays a fascinating array of physical properties such as decreasing solubility with temperature or phase separation under specific solvent conditions, *i.e.* controlling ionic strength and/or temperature[1–6]. It is for these reasons that PEG and other non-ionic water-soluble polymers, such as poly N-isopropylacrylamide (PNiPAM), have already gained wide uses in

biomedical, pharmaceutical, coating, and other industrial applications[7–9].

Previous studies have reported on grafted gold nano particles with PEG (PEG-AuNPs) and detailed their assembly in two and three dimensional superlattices, as driven by a variety of suspension conditions[10–22]. Recently, we reported columnar phases of PEG-AuNP nanorods with lattice constants that shrink with increasing temperature, thus suggesting that these materials have negative thermal expansion (NTE) coefficients[23]. In this study, we report on the properties of spherical PEG-AuNPs assembled into superlattices and show that, they have NTE properties. We unravel the underlying mechanism and, in this way, expand the range of physical properties attainable in nanoparticle assemblies and broaden the reach of NTE materials.

The (volumetric) coefficient of thermal expansion is defined as

$$\begin{aligned} \alpha_V &= \frac{1}{V}\left(\frac{\partial V}{\partial T}\right)_{P,N} = 3\frac{\partial \log(a_L(T,P))}{\partial T} \\ &= -\frac{1}{V}\left(\frac{\partial S}{\partial P}\right)_{T,N} = \frac{1}{B}\left(\frac{\partial S}{\partial V}\right)_{T,N} \end{aligned} \quad (1)$$

(Note that $V \propto a_L(T,P)^3$ which leads to the top rhs), where the top rhs of the equation applies to a crystal whose lattice constant, as a function of temperature (T) and pressure (P), is given by $a_L(T,P)$, the lattice constant. The bottom equations follow from Maxwell relations and indicate that if $\alpha < 0$ entropy is an increasing function with pressure or decreasing with volume (since $B > 0$ is the bulk modulus). In most of nanoparticle superlattices reported to date, α_V has been shown to be positive, *e.g.* alkylthiolated[24] or DNA[25] functionalized nanoparticles. NTEs of isotropic materials are rare[26,27], perhaps water is the most common NTE system in the $0-4$ °C range. Other remarkable cases are crystals, such as zirconium tungstate ZrW_2O_8[28] or the perovskite ScF_3[29,30]. A grazing incidence small angle X-ray scattering study on PNiPAM-based nanoparticle system shows negligible NTE properties, and stronger dependence on relative humidity[31]. Expanding the realm of NTEs into nanoparticle materials opens potential new applications in sensing, catalysis, energy storage and conversion, plasmonics and optoelectronics[32–35].

Methods

Our experimental system consists of spherical AuNPs of 10 nm in diameter that are grafted with PEG by ligand-exchange[10,11]. Briefly, polyethylene glycol methyl ether thiol of either molecular weight (M_n) of $\sim$ 2 or $\sim$ 5 kDa (henceforth referred to as PEG2k and PEG5k, respectively) is added to citrate-stabilized AuNP suspensions with a molar ratio of 6000 : 1 (PEG to AuNP), and incubated for $\sim$ 3 days under rota-shaking. The mixture (PEG + AuNPs) is purified three times through centrifuging at 21000 g for 90 min to eliminate the unbound PEG and then redispersed in ultrapure water for $\sim$ 15 nM concentration of PEG-AuNPs. Grafting of PEG on the AuNPs is confirmed by comparing the hydrodynamic diameter of bare AuNPs and PEG-AuNPs obtained by dynamic light scattering (DLS) (Fig. S1).

To determine the 3D structural properties of the assembled PEG-AuNPs, synchrotron small angle X-ray scattering (SAXS)experiments were conducted at beamline 12ID-B of the Advanced Photon Source at Argonne National Laboratory (X-ray energy, 13.3 keV)[36]. Experimental samples were loaded in thin-wall quartz capillaries and measured in the temperature range $20-80$ °C. During heating and cooling, temperature is increased in steps of 10 °C/min, and SAXS measurements are collected 10 min after temperature readout is reached. The SAXS measurements and analysis follow established procedures[11,23].

Results and Discussion

Figure 1 shows structure factor profiles, $S(Q)$ (obtained by dividing the SAXS intensity by the form factor of a AuNP, see Fig. S2, and more details on the extraction of $S(Q)$ in the SI) of PEG5k-AuNPs in the presence of 500

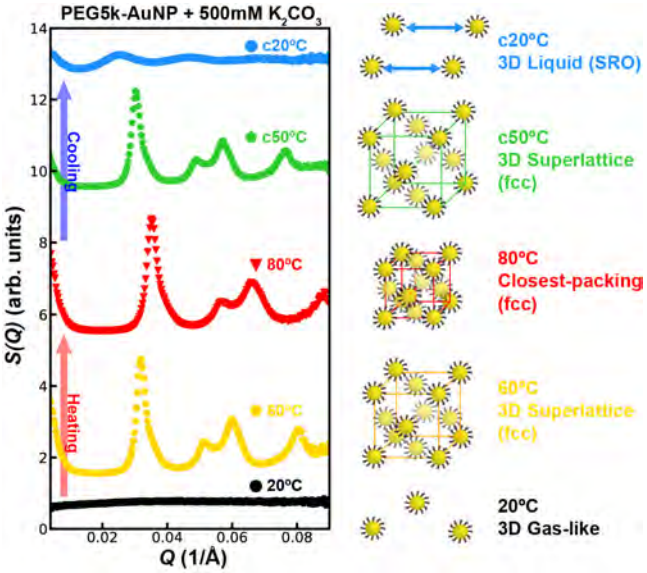

Figure 1: Diffraction patterns ($S(Q)$) of PEG5k-AuNPs suspension at 500 mM K_2CO_3 at various temperatures. At 20 °C, no features are observed in the structure factor (S(Q)) profile of PEG5k-AuNPs, indicating well-dispersed NPs in the bulk (3D gas-like phase). High order diffraction peaks appear at $T \approx 60$ °C and shift to larger Q values as the temperature is increased to 80 °C, indicating ordered 3D assemblies are formed with a tendency toward a closer packing as temperature is increased. As temperature is decreased back to 20 °C, the fundamental peak shifts to lower Q values, evidence of larger unit cell. The distinctive multiple diffraction peaks are not observed below the 50 °C, but remain intense (3D liquid-like, short range order (SRO)), reflecting the irreversibility of assemblies. Scans labeled with prefix 'c' indicate they were performed after cooling from 80 °C. The structure factor profiles upon heating and cooling are vertically shifted for clarity.

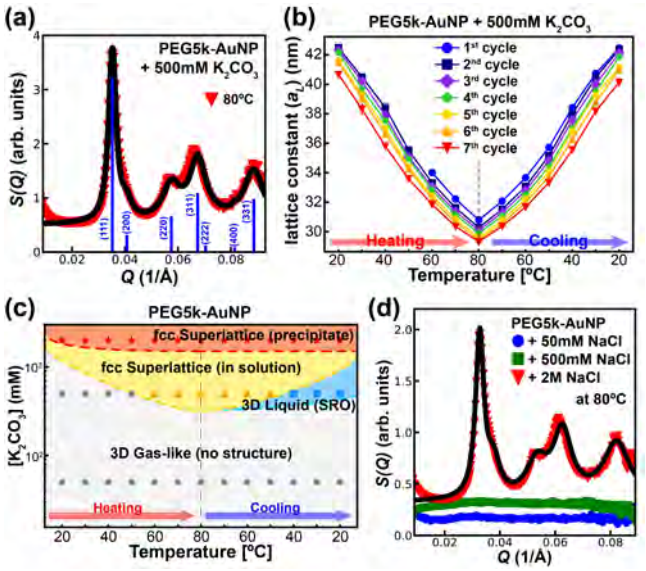

Figure 2: (a) Structure factor (S(Q)) profile for assemblies of PEG5k-AuNPs with 500 mM K_2CO_3 at 80 °C and its corresponding best-fit profiles (black solid line) using ideal fcc model structure. Vertical lines indicate relative intensities at the fcc peak positions. (b) fcc lattice constant ($a_L = \sqrt{12}\pi/Q_1$, Q_1 is the fundamental diffraction peak) for assemblies of PEG5k-AuNPs with 500 mM K_2CO_3 at various temperatures. The temperature of the sample is raised from 20 °C to 80 °C (heating), and then lowered back to 20 °C (cooling). (c) Phase diagram of PEG5k-AuNPs as functions of K_2CO_3 concentration and temperature. The markers (circles, triangles, squares and stars) indicate 3D gas-like, fcc superlattice in solution, 3D liquid (SRO) and precipitated fcc superlattice. The phase boundary dash lines are not exact and are speculated based on the limited experimental data sets. (d) Structure factor (S(Q)) profiles for PEG5k-AuNP suspensions at various concentrations of NaCl as indicated, at 80 °C. Black solid line is the best-fit profile using fcc model structure.

mM K_2CO_3 upon heating and cooling. Initially at 20 °C, S(Q) is featureless as expected from well dispersed PEG5k-AuNPs in the aqueous suspension. However, above $\sim$ 50 °C, S(Q) exhibits noticeable diffraction peaks arising from ordered assemblies of PEG5k-AuNPs at $\sim$ 60 °C. Increasing the temperature further leads to a uniform shift of the peaks to larger Q values, indicating contraction of the lattice. This temperature induced ordering is further accompanied by improved crystal-quality, as the diffraction peaks sharpen upon heating (crystal quality is discussed in the SI, see Fig. S3)[37–39]. The diffraction peaks at high temperature can be indexed as face centered cubic (fcc) by using ideal fcc lattice structure factor model with Lorentzian function peak-shape (fitting profile in Fig. 2(a)). Upon cooling down from 80 °C, the diffraction peaks shift to lower Q values, indicating a larger unit cell in PEG-AuNP assemblies. Below $\sim$ 40 °C, the diffraction peaks broaden significantly but the fundamental diffraction peak (Q_1) remains,

consistent with short-range ordered (SRO) PEG5k-AuNPs, pointing to the irreversibility induced by temperature assembly, at least on time scales of the conducted experiments (*i.e.,* a few hours).

The robustness of the assembly process is further demonstrated through multiple heating/cooling cycles. As shown in Fig. 2(b), fcc lattice constant ($a_L = \sqrt{12}\pi/Q_1$, Q_1 indicates the fundamental diffraction peak) becomes smaller and larger under repeated heating and cooling cycles, respectively, signifying high thermal stability and tunable packing density (see also Fig. S4). Notwithstanding, slight out-of-equilibrium effects are present, as consecutive temperature cycles incrementally reduce the lattice constant, reaching a minimum at 80 °C in the 7$^{\text{th}}$ cycle. The lattice constant (a_L) versus temperature (upon heating and cooling) is approximately linear and the slope trends like the thermal expansion coefficient (α_V) from Eq. (1), with $\sim -1,71 \times 10^{-2}\text{K}^{-1}$, independent of temperature at $P = 1$ atm. The multiple thermal cycles gradually create precipitations of PEG-AuNP, that lower the concentration of the aggregated superstructures in the suspension, causing a decrease in diffraction peak height. Regardless, the fcc S(Q) profiles persist even to the 7th cycle (see Fig. S5).

In addition to temperature, PEG5k-AuNP assembly is sensitive to salt (K_2CO_3) concentration (more details in SI and Figs. S6−S8). At low concentrations (below $\sim$ 50 mM) there is no assembly, while at high K_2CO_3 concentration ($\sim$ 2 M), fcc superlattices become large and precipitate (see Fig. S17). Our results are summarized in a phase diagram as a function of K_2CO_3 concentration and temperature, Fig. 2(c). The importance of electrolyte and temperature effects for the PEG-AuNP assemblies is extensively confirmed with various control experiments in ultrapure water without salts that do not show assembly and ordering (Fig. S9).

The universality of the effect is also demonstrated by other salts (NaCl, instead of K_2CO_3) and PEG lengths. At 2 M NaCl, PEG5k-AuNPs assemble into fcc at high temperature (80 °C), but require higher salt concentration and temperature compared to K_2CO_3 (Figs. 2(d), S10, and S11), and the NTE coefficient remains negative (see Table 1). The K_2CO_3 is more effective than NaCl in inducing assemblies of PEG5k-AuNPs, following the Hofmeister series as demonstrated previously[12]. Table 1 and Figs. S12−S16, show that PEG with different lengths do not alter the NTE behavior, but modify the value of actual lattice constants. Evaluating the full-width at half maximum (fwhm) provides the average crystalline size $l_{SL} \approx 2\pi/\text{fwhm}$, with $l_{SL} \geq 150$ nm for PEG5k-AuNP with 500 mM K_2CO_3 (see Table S1). The number of AuNPs in the fcc crystal is about one thousand under optimal conditions of PEG5k, 500 mM K_2CO_3, see Fig. S18.

In the absence of salt, PEG is water soluble with an effective Flory-Huggins parameter $\chi \leq \frac{1}{2}$[2] for which no assembly is possible. The addition of salt reduces the effective number of water molecules available (as some are bound in hydration layers around the ions) and in this way drive PEG insolubility ($\chi > \frac{1}{2}$). We provide a simplified calculation for χ based on a single PEG-AuNP with $\mathcal{N}_p$ PEG chains (a spherical brush). The free energy consists of mixing and stretching terms[40,41]:

Table 1: fcc lattice constant (a_L) and coefficient of thermal expansion (α_V) for PEG-AuNPs of different PEG lengths and solvent conditions.

Nano-particle	Salt	Temperature (n^{th} Cycle)	a_L[1] (nm)	α_V[2] ($\cdot 10^{-2}$ K^{-1})
PEG5k-AuNP	K_2CO_3*	80 °C (1$^{\text{st}}$)	30.79(3)	−1.71
	K_2CO_3	80 °C (7$^{\text{th}}$)	29.32(2)	
	NaCl**	80 °C (1$^{\text{st}}$)	33.15(3)	−1.20
PEG2k-AuNP	K_2CO_3	80 °C (1$^{\text{st}}$)	28.13(1)	−0.89
	K_2CO_3	80 °C (5$^{\text{th}}$)	27.91(1)	

[1] fcc lattice constant, $a_L = \sqrt{12}\pi/Q_1$.

[2] coefficient of thermal expansion from Eq. (1) (at P=1 atm).

* all [K_2CO_3] = 500 mM.

** [NaCl] = 2 M.

$$\frac{F}{k_B T} = \int_0^H \frac{dz}{v} S_d(R+z) \times \left[(1-\phi(z)) \log\left(\frac{1-\phi(z)}{e}\right) + 1 + \chi\phi(z)\,(1-\phi(z)) \right] + \frac{\mathcal{N}_p}{c_s b} \int_0^H dz \frac{dz}{dN} \tag{2}$$

where $\phi(z)$ is the polymer distribution at a distance z from the core, H is the PEG shell thickness, N is the number of Kuhn monomers, R the core radius, $S_d(x)$ a geometric factor ($= 4\pi x^2$ for PEG-AuNPs), b the Kuhn length, c_s is a coefficient ($c_s = \frac{2}{3}$), and χ is the Flory-Huggins parameter between PEG and solution, see SI Table S2, for actual values and additional details. In the SI, Eq. (S4) and following equations, we obtain the polymer thickness H as a function of χ, shown in Fig. 3, see also Fig. S20.

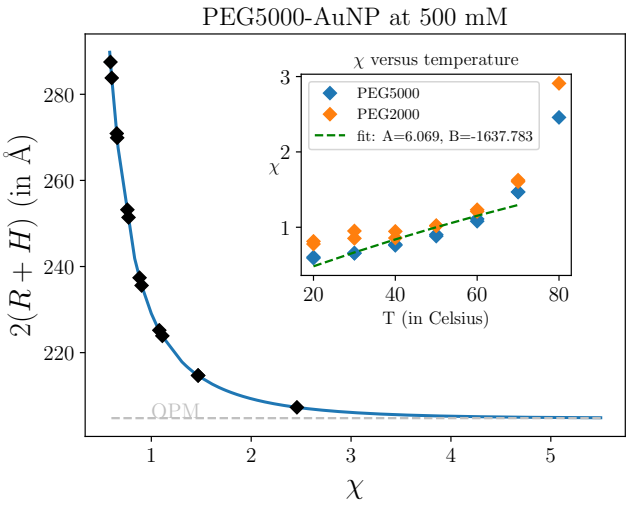

Figure 3: Dependence of the nanoparticle diameter $2(R+H)$ as a function of χ, with the other values as in Table S2. The black diamonds are the experimental results from Eq. (3). In the inset we show the dependence of the Flory-Huggins parameter χ, see Eq. (2), with temperature at 500 mM, with the values as described in Table S2. The green dashed line is a fit to $\chi = A + B/T$

The quantity $2(R+H)$ defines the equivalent hard sphere diameter of the nanoparticle[42]. For the fcc superlattice of optimally packed hard spheres, the nearest neighbor D_n is

$$D_n \equiv 2(R+H)\ . \tag{3}$$

Relating the hard sphere diameter of a single nanoparticle with the lattice constant of the fcc superlattice has been rigorously shown to apply for polystyrene[43] and alkylthiolated nanoparticles[44] systems. The hard sphere diameter as a function of χ is shown in Fig. 3 and converges to the optimal packing model (OPM) result[24] corresponding to the non-solvent case. Using Eq. (3) and the neighbor distance D_n for the experiment, see Table S1 for the exact values at 500 mM, the values of the Flory-Huggins parameters are obtained for each temperature, see Fig. 3 (and also Fig. S21 for PEG2000).

In the inset of Fig. 3 we show the explicit dependence of χ on temperature. It is reassuring that the values are roughly independent of polymer length. A fit to the empirical form $\chi = A + B/T$ is only partially successful, but this is expected, given that the Flory-Huggins parameter includes contributions from hydrogen bonds and ionic strength[2].

The interpretation of the results at the molecular level is that the presence of salt creates hydration layers around ions, which in turn reduces the number of "free" water molecules, *i.e.,* that associate with PEG. This competition for free water molecules leas to PEG insolubility $\chi > \frac{1}{2}$. As the temperature is increased the solubility is decreased even further by two effects: enhanced hydrophobicity of the -CH_2 groups[2] and also, the decrease of water dielectric constant, which makes the binding to ions stronger. This, explains the reduction of superlattice volume and increase in entropy, thus illustrating the content of the thermodynamic identity Eq. (1), as well as the enhancement of the Flory-Huggins parameter. This is illustrated in Fig. 4. As a crosscheck we show, see Eq. (S40), that the observed order of magnitude for α_V follows from the proposed mechanism.

From Eq. 1 it is

$$\Delta S \approx B\alpha\Delta V\ , \tag{4}$$

thus in NTE materials $\alpha < 0$, a decrease of volume implies an increase in entropy,

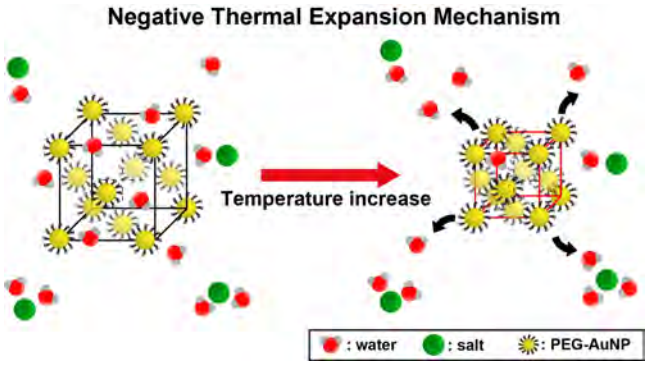

Figure 4: Illustration of the NTE mechanism for a PEG-AuNP superlattice (not to scale). For clarity, salts are not distinguished by positive and negative ions, and the bulk water is omitted.

since the bulk modulus B is positive as it follows from thermodynamic stability conditions. The mechanism in previous NTE materials[27] consists of atoms connected by strong bonds but with unconstrained (floppy) motions such that nearest neighbors are maximally separated at low temperatures. As temperature is increased, atoms vibrate out of the maximal separation becoming, on average, closer together, *i.e.* the shrinking of the nearest neighbor distances occurs because of an increase in vibrational entropy leading to $|\alpha_V| \approx 10^{-5} - 10^{-6}\mathrm{K}^{-1}$, with $CO_3[Co(CN)_6]_2$ reaching $|\alpha_V| \approx 10^{-4}$[27]. The mechanism for NTE superlattices, see Fig. 4, is obviously different, as the source of entropy increase is the unbinding of water molecules as driven by the hydrophobicity of the backbone components, leading to NTE coefficients that are between 2-4 orders of magnitude larger (in magnitude). In SI (Eq. S37 and beyond) we provide an estimate that the order of the effects are consistent with the measured value of α.

Conclusions

In summary, our study shows that PEG-AuNP superlattices assembled by salt have NTE properties by a distinct mechanism, where the hydrophobic moieties of the polymer induce a conformation change, decreasing the lattice constant while increasing the entropy. Further studies are required to establish what determines crystal size. The values of the Flory-Huggins parameter in Fig. 3 imply that the small size soluble superlattices, see Fig. 2(c), should become unstable against the formation of a large superlattice and precipitate, as found for higher salt concentrations (see discussion following Eq. (S31)). A more complete model, with specific treatment of hydrogen bonds as done in Ref.[2] is necessary to address crystal size.

Associated Content

Supporting Information

The Supporting Information is available free of charge on the ACS Publications website at DOI:

The Supporting information includes the following: 1) Characterization of PEG-AuNPs by using DLS and SAXS 2) SAXS data for PEG5k- and PEG2k-AuNPs with K_2CO_3 under thermal controls 3) SAXS data for PEG5k- and PEG2k-AuNP in ultrapure water 4) SAXS data for PEG5k-AuNPs with NaCl under thermal controls 6) Theoretical model for free energy of a spherical brush 7) Model predictions for lattice constant and superlattice sizes 7) Order of magnitude estimate of α_V.

Author information

*(A.T.) email: trvsst@ameslab.gov
*(D.V.) email: vaknin@ameslab.gov

Acknowledgments

We thank the beamline staff team at 12ID-B for synchrotron beamline support at the Advanced Photon Source (APS), Argonne National Laboratory. Research was supported by the U.S. Department of Energy (U.S. DOE), Office of Basic Energy Sciences, Division of Materials Sciences and Engineering. Ames Laboratory is operated for the U.S. DOE by Iowa State University under Contract DE-AC02-07CH11358. Use of the Advanced Photon Source, an Office of Science User Facility operated for the U.S. DOE Office of

Science by Argonne National Laboratory, was supported by the U.S. DOE under Contract DE-AC02-06CH11357.

References

1. Matsuyama, A.; Tanaka, F. Theory of Solvation-Induced Reentrant Phase Separation in Polymer Solutions. *Phys. Rev. Lett.* **1990**, *65*, 341–344.

2. Dormidontova, E. E. Role of Competitive PEO- Water and Water- Water Hydrogen Bonding in Aqueous Solution PEO Behavior. *Macromolecules* **2002**, *35*, 987–1001.

3. Huddleston, J. G.; Willauer, H. D.; Rogers, R. D. Phase Diagram Data for Several PEG + Salt Aqueous Biphasic Systems at 25 C. *J. Chem. Eng. Data* **2003**, *48*, 1230–1236.

4. Walter, H.; Brooks, D. E.; Fisher, D. *Partitioning in Aqueous Two-Phase Systems*; Academic Press: New York, 1985.

5. Saeki, S.; Kuwahara, N.; Nakata, M.; Kaneko, M. Upper and Lower Critical Solution Temperatures in Poly (ethylene glycol) Solutions. *Polymer* **1976**, *17*, 685–689.

6. Tanaka, F. Theoretical Study of Molecular Association and Thermoreversible Gelation in Polymers. *Polym. J.* **2002**, *34*, 479–509.

7. Veronese, F. M.; Pasut, G. PEGylation, Successful Approach to Drug Delivery. *Drug Discovery Today* **2005**, *10*, 1451–1458.

8. Jagur-Grodzinski, J. Polymeric Gels and Hydrogels for Biomedical and Pharmaceutical Applications. *Polym. Adv. Technol.* **2010**, *21*, 27–47.

9. Guan, Y.; Zhang, Y. PNIPAM Microgels for Biomedical Applications: from Dispersed Particles to 3D Assemblies. *Soft Matter* **2011**, *7*, 6375–6384.

10. Zhang, H.; Wang, W.; Mallapragada, S.; Travesset, A.; Vaknin, D. Macroscopic and Tunable Nanoparticle Superlattices. *Nanoscale* **2017**, *9*, 164–171.

11. Zhang, H.; Wang, W.; Akinc, M.; Mallapragada, S.; Travesset, A.; Vaknin, D. Assembling and Ordering Polymer-Grafted Nanoparticles in Three Dimensions. *Nanoscale* **2017**, *9*, 8710–8715.

12. Zhang, H.; Wang, W.; Mallapragada, S.; Travesset, A.; Vaknin, D. Ion-Specific Interfacial Crystallization of Polymer-Grafted Nanoparticles. *J. Phys. Chem. C* **2017**, *121*, 15424–15429.

13. Wang, W.; Zhang, H.; Mallapragada, S.; Travesset, A.; Vaknin, D. Ionic Depletion at the Crystalline Gibbs Layer of PEG-Capped Gold Nanoparticle Brushes at Aqueous Surfaces. *Phys. Rev. Mater.* **2017**, *1*, 076002.

14. Nayak, S.; Horst, N.; Zhang, H.; Wang, W.; Mallapragada, S.; Travesset, A.; Vaknin, D. Interpolymer Complexation as a Strategy for Nanoparticle Assembly and Crystallization. *J. Phys. Chem. C* **2018**, *123*, 836–840.

15. Nayak, S.; Fieg, M.; Wang, W.; Bu, W.; Mallapragada, S.; Vaknin, D. Effect of (Poly) electrolytes on the Interfacial Assembly of Poly (ethylene glycol)-Functionalized Gold Nanoparticles. *Langmuir* **2019**, *35*, 2251–2260.

16. Kim, H. J.; Wang, W.; Bu, W.; Hossen, M. M.; Londono-Calderon, A.; Hillier, A. C.; Prozorov, T.; Mallapragada, S.; Vaknin, D. Salt Mediated Self-Assembly of Poly (ethylene glycol)-Functionalized Gold Nanorods. *Sci. Rep.* **2019**, *9*, 1–9.

17. Wang, W.; Kim, H. J.; Bu, W.; Mallapragada, S.; Vaknin, D. Unusual Effect of Iodine Ions on the Self-Assembly of Poly (ethylene glycol)-Capped Gold Nanoparticles. *Langmuir* **2019**, *36*, 311–317.

18. Kim, H. J.; Hossen, M. M.; Hillier, A. C.; Vaknin, D.; Mallapragada, S. K.; Wang, W. Interfacial and Bulk Assembly of Anisotropic Gold Nanostructures: Implications for Photonics and Plasmonics. *ACS Appl. Nano Mater.* **2020**, *3*, 8216–8223.

19. Kim, H. J.; Wang, W.; Mallapragada, S. K.; Vaknin, D. The Effects of Temperature on the Assembly of Gold Nanoparticle by Interpolymer Complexation. *J. Phys. Chem. Lett.* **2021**, *12*, 1461–1467.

20. Choueiri, R. M.; Klinkova, A.; Thérien-Aubin, H.; Rubinstein, M.; Kumacheva, E. Structural Transitions in Nanoparticle Assemblies Governed by Competing Nanoscale Forces. *J. Am. Chem. Soc.* **2013**, *135*, 10262–10265.

21. Zámbó, D.; Radnóczi, G. Z.; Deák, A. Preparation of Compact Nanoparticle Clusters from Polyethylene Glycol-Coated Gold Nanoparticles by Fine-Tuning Colloidal Interactions. *Langmuir* **2015**, *31*, 2662–2668.

22. Schroer, M. A.; Lehmkühler, J., Felix a Möller; Lange, H.; Grübel, G.; Schulz, F. Pressure-Stimulated Supercrystal Formation in Nanoparticle Suspensions. *J. Phys. Chem. Lett.* **2018**, *9*, 4720–4724.

23. Kim, H. J.; Wang, W.; Travesset, A.; Mallapragada, S. K.; Vaknin, D. Temperature-Induced Tunable Assembly of Columnar Phases of Nanorods. *ACS nano* **2020**, *14*, 6007–6012.

24. Landman, U.; Luedtke, W. D. Small Is Different: Energetic, Structural, Thermal, and Mechanical Properties of Passivated Nanocluster Assemblies. *Faraday Discuss.* **2004**, *125*, 1–22.

25. Xiong, H.; van der Lelie, D.; Gang, O. Phase Behavior of Nanoparticles Assembled by DNA Linkers. *Phys. Rev. Lett.* **2009**, *102*, 15504.

26. Lind, C. Two Decades of Negative Thermal Expansion Research: Where Do We Stand? *Materials* **2012**, *5*, 1125–1154.

27. Dove, M. T.; Fang, H. Negative Thermal Expansion and Associated Anomalous Physical Properties: Review of the Lattice Dynamics Theoretical Foundation. *Rep. Prog. Phys.* **2016**, *79*, 066503.

28. Mary, T. A.; Evans, J. S.; Vogt, T.; Sleight, A. W. Negative Thermal Expansion from 0.3 to 1050 Kelvin in ZrW2O8. *Science* **1996**, *272*, 90–92.

29. Greve, B. K.; Martin, K. L.; Lee, P. L.; Chupas, P. J.; Chapman, K. W.; Wilkinson, A. P. Pronounced Negative Thermal Expansion from a Simple Structure: Cubic ScF3. *J. Am. Chem. Soc.* **2010**, *132*, 15496–15498.

30. Wendt, D.; Bozin, E.; Neuefeind, J.; Page, K.; Ku, W.; Wang, L.; Fultz, B.; Tkachenko, A. V.; Zaliznyak, I. A. Entropic Elasticity and Negative Thermal Expansion in a Simple Cubic Crystal. *Sci. Adv.* **2019**, *5*, eaay2748.

31. Li, B.; Smilgies, D.-M.; Price, A. D.; Huber, D. L.; Clem, P. G.; Fan, H. Poly (N-isopropylacrylamide) Surfactant-Functionalized Responsive Silver Nanoparticles and Superlattices. *ACS nano* **2014**, *8*, 4799–4804.

32. Yi, C.; Yang, Y.; Liu, B.; He, J.; Nie, Z. Polymer-Guided Assembly of Inorganic Nanoparticles. *Chem. Soc. Rev.* **2020**, *49*, 465–508.

33. Fan, J. A.; Wu, C.; Bao, K.; Bao, J.; Bardhan, R.; Halas, N. J.; Manoharan, V. N.; Nordlander, P.; Shvets, G.; Capasso, F. Self-Assembled Plasmonic Nanoparticle Clusters. *Science* **2010**, *328*, 1135–1138.

34. Boles, M. A.; Engel, M.; Talapin, D. V. Self-Assembly of Colloidal Nanocrystals: from Intricate Structures to Functional

Materials. *Chem. Rev.* **2016**, *116*, 11220–11289.

35. Sun, L.; Lin, H.; Kohlstedt, K. L.; Schatz, G. C.; Mirkin, C. A. Design Principles for Photonic Crystals Based on Plasmonic Nanoparticle Superlattices. *Proc. Natl. Acad. Sci.* **2018**, *115*, 7242–7247.

36. The 12-ID-B beamline at the Advanced Photon Source (APS), Argonne National Laboratory. https://12id.xray.aps.anl.gov/ (accessed April 6, 2021).

37. Zhang, J.; Santos, P. J.; Gabrys, P. A.; Lee, S.; Liu, C.; Macfarlane, R. J. Self-Assembling Nanocomposite Tectons. *J. Am. Chem. Soc.* **2016**, *138*, 16228–16231.

38. Santos, P. J.; Cheung, T. C.; Macfarlane, R. J. Assembling Ordered Crystals with Disperse Building Blocks. *Nano Lett.* **2019**, *19*, 5774–5780.

39. Abdilla, A.; Dolinski, N. D.; de Roos, P.; Ren, J. M.; van der Woude, E.; Seo, S. E.; Zayas, M. S.; Lawrence, J.; Read de Alaniz, J.; Hawker, C. J. Polymer Stereocomplexation as a Scalable Platform for Nanoparticle Assembly. *J. Am. Chem. Soc.* **2020**, *142*, 1667–1672.

40. Wijmans, C. M.; Zhulina, E. B. Polymer Brushes at Curved Surfaces. *Macromolecules* **1993**, *26*, 7214–7224.

41. Rubinstein, M.; Colby, R. H., *et al. Polymer physics*; Oxford University Press: New York, 2003; Vol. 23.

42. Zha, X.; Travesset, A. The Hard Sphere Diameter of Nanocrystals (Nanoparticles). *J. Chem. Phys.* **2020**, *152*, 094502.

43. Xia, J.; Horst, N.; Guo, H.; Travesset, A. Superlattices of Nanocrystals with Polystyrene Ligands: From the Colloidal to Polymer Limit. *Macromolecules* **2019**, *52*, 8056–8066.

44. Zha, X.; Travesset, A. Stability and Free Energy of Nanocrystal Chains and Superlattices. *J. Phys. Chem. C* **2018**, *122*, 23153–23164.